Materials Today Communications 35 (2023) 106291

Contents lists available at ScienceDirect

Materials Today Communications

journal homepage: www.elsevier.com/locate/mtcomm

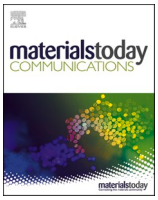

Phase equilibria in the Ti-Al-W system between 800 and 1300 °C

B. Distl [a,*], B. Rashkova [b], F. Stein [a,*]

[a] Max-Planck-Institut für Eisenforschung GmbH, Düsseldorf, Germany
[b] Montanuniversität Leoben, Leoben, Austria

ARTICLE INFO

Keywords:
Phase equilibria
Reaction schematic
Microstructure
Isothermal sections

ABSTRACT

Within the search for new improved high-temperature materials for gas turbine applications with higher energy saving potential and improved greenhouse gas balance, new Ti-Al-W based alloys have recently been discussed. A basic prerequisite for targeted alloy development is the precise knowledge of the phases and phase relationships that determine the microstructure and mechanical behavior of the material. However, there is not much known about the phase equilibria in the application- and manufacturing-relevant temperature range between 800 and 1300 °C. No information on ternary intermetallic compounds or possible ordering of the cubic (βTi,W) solid solution is reported in the literature. In the present investigation, the Ti-rich part of the Ti–Al–W system between 800 and 1300 °C was studied. Ten different alloys were heat-treated and quenched samples were characterized by scanning electron microscopy (SEM), electron probe microanalysis (EPMA), high-energy XRD (HEXRD), differential thermal analysis (DTA), and transmission electron microscopy (TEM). Based on these results, a series of partial isothermal sections was established. The investigations show that there is no ternary intermetallic compound in this system and the (W) solid solution forms equilibria with the binary Ti-Al phases.

1. Introduction

In the last decades, several TiAl-based alloys with tungsten (W) as an alloying element were developed for use in high-temperature structural applications. The so-called "ABB-alloy" (Ti-47Al-2W-0.5Si); all composition data here and in the following in at% was developed for investment casting and showed promising creep properties at 760 °C, but the ductility at room temperature was poor [1]. The alloy G4 (Ti-47Al-1Re-1 W-0.2Si) [2] is a further development of the ABB alloy, which has even better creep properties, but whose liability to casting defects leads to very inhomogeneous and unpredictable mechanical properties [3]. Therefore, a spark-plasma sintering route has been explored for this alloy, showing promising results [4]. In addition, the so-called IRIS alloy (Ti-48Al-2 W-0.08B) has also been developed for this process route. This alloy shows promising mechanical properties to achieve application temperatures above 800 °C [4–11]. Through the development of the above-mentioned alloys, W has been identified as another promising (βTi)-stabilizing alloying element (besides Nb and Mo) for 3rd generation TiAl-based alloys [12]. However, experimental studies of the Ti–Al–W system and its phase equilibria are very limited and mostly focus on specific, restricted composition regions or single alloys in this ternary system [13–18].

The Ti-rich corner of the Ti–Al–W system (up to maximum Al and W contents of about 30 and 5 at%, respectively) has been studied by Oleynikova et al. [13] at 600, 800, 1000, and 1100 °C in the 1970 s with a series of alloys "highly contaminated with carbon" [13], which casts some doubt on the accuracy of these results. Moreover, no phase compositions were measured in this study and the reported respective values are only estimates. These studies reveal that (βTi) shows a considerable solubility for Al at 1100 °C (estimated as ~17 at%). At lower temperatures, there are indications for different three-phase equilibria between the (W) solid solution and (αTi), (βTi), and Ti_3Al. The solubility of W in (αTi) and Ti_3Al was estimated as ~0.4 at% between 800 and 1100 °C. The work of Sparks et al. [14] deals with the effect of ternary additions to the Al-rich compound $TiAl_3$. After heat treatment of an alloy with nominal composition Ti-63Al-12 W at 1200 °C, they found a three-phase equilibrium between $TiAl_3$, the (W) solid solution, and a third phase with an approximate composition Ti-68Al-4 W. The crystal structure was identified as cubic $L1_2$-type, but it cannot be ruled out that this phase was confused with the Al-rich TiAl (γ) phase, which exists in the binary system up to 72 at% Al [19,20].

Since then, there have been only a few further studies, all of which focus on specific phase equilibria above 1000 °C in alloys with application-relevant compositions between 44 and 48 at% Al [15–18]. Since all these alloys have fairly low contents of W, there is not much known about the phase equilibria in the ternary composition triangle. In

* Corresponding authors.

https://doi.org/10.1016/j.mtcomm.2023.106291
Received 28 April 2023; Received in revised form 18 May 2023; Accepted 22 May 2023
Available online 23 May 2023

addition to that, there is a partial liquidus projection reported by Jung et al. [21] based on directional solidification experiments, confirming the (βTi)-stabilizing effect of W. Besides the $L1_2$-type phase observed by Sparks et al. [14], there is no report of a ternary intermetallic compound in the literature. The scarcity of data emphasises the need for further experimental investigations within this system in order to determine the phase equilibria over a wider composition and temperature range.

In the present work the phase equilibria in the Ti–Al–W system were investigated with a series of Ti-Al-rich ternary alloys heat-treated between 800 and 1300 °C. The alloys were characterized by means of scanning electron microscopy (SEM), electron probe microanalysis (EPMA), high-energy XRD (HEXRD), differential thermal analysis (DTA), and transmission electron microscopy (TEM). Six partial isothermal sections are established based on the measured data, and the results are discussed in the context of the information available from the above-mentioned literature. For the binary boundary systems, the phase diagrams reported in Refs. [19,20] (Ti–Al), [22] (Ti–W), and [23] (Al–W) were used. The crystallographic information about the phases observed in the investigated alloys of the present study are summarized in Table 1. The two bcc phases βTi and W are completely miscible at high temperatures (>1250 °C [22]), which is why the resulting continuous solid solution is referred to as (βTi,W) in the following. The results of the present work aim to provide an improved and more comprehensive picture of the Ti–Al–W system and to clarify open questions such as the existence/non-existence of a ternary intermetallic compound and the occurrence of phase equilibria between Ti-Al phases and the W solid solution.

2. Experimental

For the alloy synthesis two different methods were used for alloy production: i) arc melting with a non-consumable tungsten electrode and tiltable crucible, ii) copper boat induction melting. To obtain high-purity alloys, the syntheses were performed in Ar atmosphere (Argon 5.0) using high-purity metals Ti (99.995 wt%), Al (99.999 wt%), and W (99.95 wt%) (HMW Hauner GmbH & Co. KG). The alloys synthesized by arc melting were cast into rod-shaped copper moulds (Ø 15 mm) resulting in samples with a length of approximately 160 mm. The rod-shaped alloys produced by induction melting had a diameter of 5 mm and a length of approximately 30 mm. To ensure chemical homogeneity, the raw materials were turned over and remolten several times in the arc and copper boat induction melting furnace. To minimize the uptake of impurities, the Ar gas was additionally dried (ZPure M™ 3800cc, Chromatography research supplies) to remove remaining moisture and oxygen. Analyzed overall compositions and impurity contents of the as-cast alloys are summarized in Table 2, and their positions in the ternary composition triangle are shown in Fig. 1. For subsequent analyses and heat treatments, the alloys were cut into pieces using a disc cutter.

In order to minimize the uptake of impurities during the heat treatments, two different setups were used depending on the heat treatment temperature. For heat treatments between 800 and 1100 °C, 10 mm long cylindrical samples were cut from the rods. Together with some Ti filings serving as oxygen getters, they were then encapsulated in fused silica ampoules, which were evacuated and backfilled with dried Ar gas. At temperatures above 1100 °C, the fused silica is no longer sufficiently gas-tight for oxygen and nitrogen [27] and the process of devitrification begins. Therefore, the "double crucible technique" [28] is used for heat treatments at 1200 and 1300 °C. The sample is wrapped with Ta foil and placed in an alumina crucible, which in turn is placed upside down in a larger crucible. The leftover space is filled with Ti filings which act as getter material. The Ta foil prevents contact between filings and the sample. Additionally, the reaction between Ta and the sample is very sluggish, so Ta was not found in any of the samples. The heat treatments were performed in an Ar atmosphere. In both cases the samples were quenched in brine by breaking the ampoules/crucibles. Using these two methods (c.f. Fig. 4 in Ref. [29]), the Ti–Al–W alloys were heat-treated between 800 and 1300 °C as summarized in Table 3.

Table 1
Crystallographic information (crystal system, Pearson symbol, space group, and Strukturbericht designation) about the phases observed in the Ti–Al–W alloys in the present study. Since the two bcc solid solutions (W) and (βTi) are completely miscible at high temperatures, the phase is designated as (βTi,W) in the following.

Phase designation	Crystal system	Pearson symbol	Space group	Strukturbericht designation	Reference
(W)	cubic	*cI*2	*Im*-3*m*	*A*2	[24]
(αTi)	hexagonal	*hP*2	$P6_3/mmc$	*A*3	[24]
(βTi)	cubic	*cI*2	*Im*-3*m*	*A*2	[24]
Ti_3Al, α_2	hexagonal	*hP*8	$P6_3/mmc$	$D0_{19}$	[25]
TiAl, γ	tetragonal	*tP*4	*P*4/*mmm*	$L1_0$	[26]

Table 2
Synthesized ternary alloys (TAW1 to TAW10) with their measured compositions (analyzed by inductively coupled plasma atomic emission spectroscopy, ICP-AES) as well as their impurity contents (O, N, C). For N, the values were all below the detection limit of 50 wt. ppm and are therefore not listed here. IM = copper boat induction melting; AM = arc melting.

Alloy No.	Synthesis method	Measured as-cast composition (ICP-AES) (at%)			Impurity contents (wt. ppm)	
		Ti	Al	W	O	C
TAW1[a]	IM	65.6	28.3	6.1	n.d.	n.d.
TAW2[a]	IM	58.1	28.8	13.1	n.d.	n.d.
TAW3	AM	58.5	40.0	1.5	125	82
TAW4	AM	57.6	40.6	1.8	215	90
TAW5	AM	53.9	45.0	1.1	250	101
TAW6	AM	53.6	45.5	0.9	385	120
TAW7[a]	IM	48.8	47.1	4.1	n.d.	n.d.
TAW8	AM	46.8	50.2	3.0	190	80
TAW9[a]	IM	42.6	50.8	6.6	n.d.	n.d.
TAW10	AM	41.8	54.9	3.3	155	64

[a] The as-cast composition was determined by EPMA grid measurements instead of ICP-AES

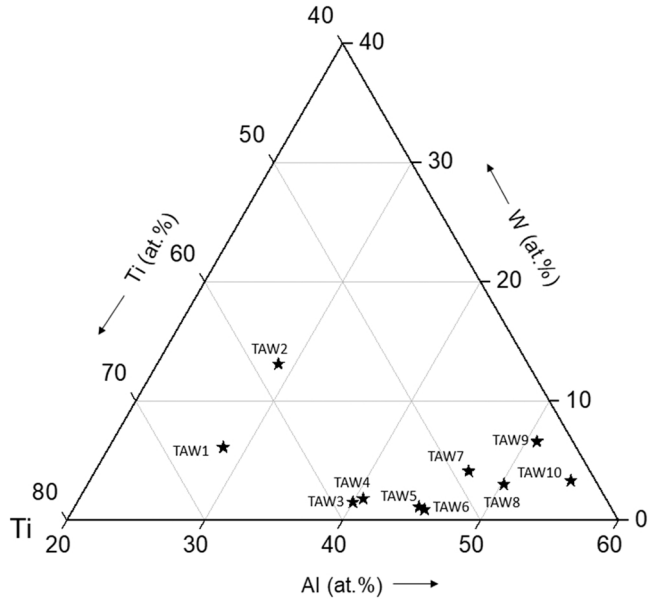

Fig. 1. As-cast alloy compositions (Table 2 2) of the ternary alloys (TAW1-TAW10) plotted in the composition triangle.

Table 3
Overview of the heat treatment times and temperatures of the ternary alloys.

Alloy No.	Heat treatment time (h)					
	Encapsulation				Double crucible technique	
	800 °C	900 °C	1000 °C	1100 °C	1200 °C	1300 °C
TAW1					30	
TAW2					30	20
TAW3						20
TAW4	2000	2000	650	400	30	20
TAW5			650	400	30	20
TAW6						20
TAW7					30	20
TAW8[a]	2000	2000	650/1300	400/800	30/60	20/40
TAW9					30	20
TAW10[a]	2000	2000	650/1300	400/800	30/60	20/40

[a] Parts of the heat-treated alloys were again heat-treated at 1000, 1100, 1200, and 1300 °C for the same time, see Section 3

After the heat treatment, the overall compositions were measured by EPMA and impurity levels of selected alloys were checked again. The oxygen content only increased slightly by less than 100 wt. ppm, while the nitrogen content remained below the detection limit of 50 wt. ppm.

The samples were hot embedded (PolyFast, Struers) and ground with 220–2500 grit abrasive SiC paper. They were then polished with polishing cloth and 3/1 μm diamond suspension before final polishing with oxide polishing suspension (OPS). The microstructures were characterized by SEM and the overall and phase compositions were determined by means of EPMA (JEOL JXY-8100) operated at an acceleration voltage of 15 kV and a probe current of 20 nA. Pure elements were used as standards. The overall compositions of the heat-treated samples were determined by grid measurements. At least three representative areas of the microstructure were measured with grids (usual step size 20 μm), each consisting of at least 196 point measurements. These measurements showed that no preferential evaporation of Al had occurred during the heat treatments. The chemical composition of the phases was determined by averaging the results of at least 12 point measurements, which were performed in different parts of the sample's cross section. In a few cases where the phases were too small for direct spot analyses (diameters ≤1 μm), the phase compositions were estimated from an extrapolation in a plot of the complete grid measurements (which were done for the determination of the overall compositions) and cross checked with TEM-EDS (energy dispersive X-ray spectroscopy) for selected alloys. Phase fractions were determined by applying the lever rule for two- and three-phase alloys to the measured values of the overall and phase compositions.

Conventional TEM was carried out using a Philips CM12 instrument operated at 120 kV. The chemical composition of the phases were measured in a Tecnai F20 operated at 200 kV by EDS microanalysis using an EDAX detector system. The Tecnai F20 was also used to take high-angle annular dark-field (HAADF) images. All specimens for TEM investigations were cut, ground, polished and subsequently electrolytically thinned to electron transparency using electrolyte A3 from Struers.

The phases were identified by room temperature HEXRD measurements with a photon energy of 100 keV (λ = 0.124 Å) and a beam size of 1 mm^2. These measurements were performed at the High-Energy Materials Science (HEMS) beamline [30] operated by Hereon at the synchrotron storage ring PETRA III, DESY, Hamburg, Germany. The data were analysed using the MAUD software package [31].

Selected alloys in the as-cast state were investigated by DTA with the aim to determine phase transformation temperatures and complement experimental results from other methods. The measurements were performed using a Netzsch DSC 404 C Pegasus thermal analyzer. For the measurements, cuboid samples with dimensions of approximately 3 × 3×2 mm were cut, cleaned with ethanol, and measured with a heating rate of 10 °C/min.

3. Results

The phase and alloy compositions determined by EPMA measurements of the ternary alloys after heat treatments at 800–1300 °C are summarized in Tables 4 to 7 along with the phase fractions determined from these measurements. The lattice parameters measured for selected alloys are summarized in Table 8. The compositions given in the following together with the alloy designations are always those measured in the as-cast condition (Table 2).

Due to the slow diffusion of W at low temperatures, equilibration of the samples especially at 800 °C proved to be very difficult, and the values given must be taken with caution (as also indicated in the corresponding Table 4).

Alloy TAW1 (Ti-28.3Al-6.1 W) was heat-treated at 1200 °C only and shows a single-phase microstructure (Fig. 2a). Based on the composition, it is concluded that this alloy is single-phase (βTi,W). For alloy TAW2 (Ti-28.8Al-13.1 W), a two-phase equilibrium between the bcc phases (βTi,W) and (W) was observed at 1200 and 1300 °C (Fig. 2b). The origin of this two-phase field is discussed below in Section 4.

The alloys TAW3 (Ti-40.0Al-1.5 W) and TAW4 (Ti-40.6Al-1.8 W) have very similar compositions resulting in nearly identical microstructures after the heat treatments. After heat treatment at 1300 °C, the microstructure is composed of the two phases (αTi) and (βTi,W) (Fig. 3a). At 1200 °C, TiAl is observed in addition in the microstructure resulting in the three-phase equilibrium (αTi) + (βTi,W) + TiAl.

Table 4
EPMA results on alloy and phase compositions as well as phase fractions of Ti–Al–W alloys heat-treated at 800 and 900 °C for 2000 h. (n.d.: not determined).

Alloy No.	Composition after heat treatment (at %)	Phases	Phase compositions measured with EPMA (at%)		Phase fraction (vol%)
			Al	W	
800 °C					
TAW4	Ti-40.6Al-1.8 W[b]	Ti_3Al	35.0 ± 1.0[d]	1.0 ± 1.0[d]	n.d.
		TiAl	45.5 ± 1.0[d]	0.5 ± 0.5[d]	n.d.
		(βTi, W)/ (W)[c]	[e]	[e]	n.d.
TAW8[a]	Ti-50.2Al-3.0 W[b]	TiAl	52.9 ± 0.6 [e]	1.2 ± 0.1 [e]	n.d.
		(W)			n.d.
TAW10[a]	Ti-54.9Al-3.3 W[b]	TiAl	56.0 ± 0.1 [e]	2.4 ± 0.1 [e]	n.d.
		(W)			n.d.
900 °C					
TAW4	Ti-40.6Al-1.8 W[b]	(βTi,W)	37.0 ± 1.0[d]	6.0 ± 1.0[d]	24
		Ti_3Al	35.0 ± 1.0[d]	0.5 ± 0.5[d]	30
		TiAl	48.0 ± 1.0[d]	0.5 ± 0.5[d]	46
TAW8[a]	Ti-50.2Al-3.0 W[b]	TiAl	51.2 ± 0.3 [e]	1.2 ± 0.1 [e]	n.d.
		(W)			n.d.
TAW10[a]	Ti-54.9Al-3.3 W[b]	TiAl	55.7 ± 0.4 [e]	2.3 ± 0.1 [e]	n.d.
		(W)			n.d.

[a] Microstructure looks similar as in the as-cast state. Therefore, it is questionable whether equilibrium was reached.
[b] As-cast composition.
[c] There is no clear experimental evidence for either (βTi,W) or (W) being the equilibrium phase in this alloy, see Section 4.1 and Fig. 7.
[d] Low accuracy because - due to fine-scaled microstructure - the values had to be estimated from grid measurements.
[e] Equilibrium composition could not be determined because the particles were too small.

Table 5
EPMA results on alloy and phase compositions as well as phase fractions of Ti–Al–W alloys heat-treated at 1000 and 1100 °C for 650 and 400 h, respectively. The values determined for alloys TAW8 and 10 were measured after prolonged heat treatment times of 1300 and 800 h, respectively (n.d.: not determined).

Alloy No.	Composition after heat treatment (at%)	Phases	Phase compositions measured with EPMA (at%)		Phase fraction (vol %)
			Al	W	
1000 °C					
TAW4	Ti-40.6Al-1.8 W[a]	(βTi, W)	35.9 ± 0.4	6.6 ± 0.7	6
		Ti_3Al	36.0 ± 0.6	0.7 ± 0.1	3
		TiAl	45.7 ± 0.5	0.5 ± 0.1	91
TAW5	Ti-44.3Al-1.1 W	(βTi, W)	35.0 ± 0.2	8.3 ± 0.3	6
		Ti_3Al	35.1 ± 0.4	0.7 ± 0.1	14
		TiAl	46.7 ± 0.3	0.6 ± 0.1	80
TAW8	Ti-51.0Al-3.1 W	TiAl	52.4 ± 0.5	1.2 ± 0.1	n.d.
		(W)	[b]	[b]	n.d.
TAW10	Ti-55.9Al-3.0 W	TiAl	57.4 ± 0.3	1.5 ± 0.2	n.d.
		(W)	[b]	[b]	n.d.
1100 °C					
TAW4	Ti-40.6Al-1.8 W[a]	(βTi, W)	36.1 ± 0.2	3.5 ± 0.1	42
		Ti_3Al	38.4 ± 0.2	0.7 ± 0.1	18
		TiAl	46.4 ± 0.2	0.5 ± 0.1	40
TAW5	Ti-44.5Al-1.1 W[a]	(βTi, W)	35.6 ± 0.5	4.1 ± 0.1	15
		Ti_3Al	37.7 ± 0.3	0.7 ± 0.1	1
		TiAl	45.9 ± 0.2	0.5 ± 0.1	84
TAW8	Ti-50.2Al-3.0 W[a]	TiAl	50.8 ± 0.4	1.1 ± 0.1	n.d.
		(W)	[b]	[b]	n.d.
TAW10	Ti-54.4Al-2.9 W	TiAl	55.4 ± 0.4	1.6 ± 0.4	n.d.
		(W)	[b]	[b]	n.d.

[a] As-cast composition. This composition was also used to determine the phase fractions.
[b] Equilibrium composition of (W) solid solution could not be determined because the particles were too small.

Table 6
EPMA results on alloy and phase compositions as well as phase fractions of Ti–Al–W alloys heat-treated at 1200 °C for 30 h. The values determined for alloys TAW8 and 10 were measured after a doubled heat treatment time of 60 h (n.d.: not determined).

Alloy No.	Composition after heat treatment (at%)	Phases	Phase compositions measured with EPMA (at%)		Phase fraction (vol %)
			Al	W	
TAW1	Ti-26.8Al-6.1 W	(βTi, W)	26.8 ± 0.2	6.1 ± 0.2	100
TAW2	Ti-28.8Al-13.1 W[a]	(βTi, W)	29.4 ± 0.5	9.9 ± 0.5	95
		(W)	0.9 ± 0.4	73.0 ± 1.6	5
TAW4	Ti-40.6Al-1.8 W[b]	(αTi)	40.6 ± 0.2	1.0 ± 0.1	47
		(βTi, W)	37.1 ± 0.3	3.6 ± 0.1	30
		TiAl	46.5 ± 0.2	0.7 ± 0.1	20
TAW5	Ti-44.5Al-1.1 W[b]	(αTi)	41.4 ± 1.4	1.0 ± 0.1	29
		(βTi, W)	37.3 ± 0.8	3.7 ± 0.1	10
		TiAl	47.2 ± 0.8	0.7 ± 0.1	61
TAW7	Ti-47.1Al-4.1 W[b]	(βTi, W)	36.0 ± 0.3	11.0 ± 0.2	19
		TiAl	48.1 ± 0.3	1.5 ± 1.5	81
TAW8	Ti-51.2Al-3.3 W	TiAl	52.4 ± 0.3	1.4 ± 0.1	n.d.
		(W)	[c]	[c]	n.d.
TAW9	Ti-48.4Al-8.4 W	TiAl	52.9 ± 1.0	2.0 ± 0.2	n.d.
		(W)	[c]	[c]	n.d.
TAW10	Ti-54.9Al-3.3 W[b]	TiAl	58.4 ± 0.4	1.9 ± 0.2	96
		(W)[d]	0.7 ± 1.2	80.8 ± 1.7	4

[a] Composition measured at 1300 °C.
[b] As-cast composition.
[c] Equilibrium composition of (W) solid solution could not be measured because the particles were too small.
[d] Phase composition determined by TEM-EDS.

Between 900 and 1100 °C (Fig. 3b), the microstructure is also three-phase, but instead of (αTi), Ti_3Al is the equilibrium phase along with (βTi,W) and TiAl in this temperature range. This is consistent with DTA measurements of these alloys which show a thermal effect at ~1130 °C that can be attributed to the first-order transition from Ti_3Al to (αTi) (similar as known from the binary system). A representative DTA measurement of alloy TAW6, which shows the same phase transitions but has a different Al content, is shown in Fig. 4.

Another important observation is that the HEXRD measurements do not show superstructure reflections of *B2*-ordering in the (βTi,W) phase, which are known to occur in related systems such as Ti–Al–Nb [29,32] and Ti–Al–Mo [33]. Also, DTA measurements of the alloys show no evidence of an order/disorder transformation of (βTi,W) in the investigated temperature range. As an example for a typical DTA curve, the results of alloy TAW6 (Ti-45.5Al-0.9 W) are shown in Fig. 4. The thermal effect observed at ~1130 °C can be associated with the first-order transition from Ti_3Al to (αTi) as already mentioned above, and the dissolution of TiAl ends close to 1290 °C. These temperatures agree with the observed changes of the microstructure and the results from the HEXRD measurements.

For the two compositionally similar alloys TAW5 (Ti-45.0Al-1.1 W) and TAW6 (Ti-45.5Al-0.9 W), large grains with a lamellar microstructure and a TiAl matrix are observed in samples quenched from 1300 °C (Fig. 5a, b). This type of lamellar (αTi) + TiAl microstructure is characteristic for Ti-Al alloys in this composition range. It should be noted that the (αTi) phase undergoes a phase transformation to Ti_3Al during cooling as a result of the eutectoid decomposition reaction (αTi) = Ti_3Al + TiAl. In the case of binary Ti-Al alloys, this eutectoid reaction takes place at 1120 °C [19,20], and the DTA measurement of TAW6 presented in Fig. 4 shows that the addition of about 1 at% W slightly shifts the reaction temperature to ~1130 °C.

The enlarged image section of the microstructure of TAW5 in Fig. 5a reveals a small amount of fine (βTi,W) phase particles that occur at the boundaries of the lamellar colonies in the 1300 °C annealed sample. Due to the very low volume fraction of this phase (< 1%), it was not detectable in HEXRD. Such (βTi,W) phase precipitates were not found in the slightly lower W alloy TAW6 (0.9 at% W compared to 1.1 at% W in TAW5) at this temperature (Fig. 5b), indicating that the addition of more than 1 at% W shifts the alloy composition at 1300 °C to the three-phase field (αTi) + (βTi,W) + TiAl. At 1200 °C, the amount of (βTi,W) phase increases as was also verified by HEXRD (Table 8). Below the eutectoid

Table 7
EPMA results on alloy and phase compositions as well as phase fractions of Ti–Al–W alloys heat-treated at 1300 °C for 20 h. The values determined for alloys TAW8 and 10 were measured after a doubled heat treatment time of 40 h (n.d.: not determined).

Alloy No.	Composition after heat treatment (at%)	Phases	Phase compositions measured with EPMA (at%)		Phase fraction (vol %)
			Al	W	
TAW2	Ti-28.8Al-13.1 W[a]	(βTi, W)	30.7 ± 0.4	10.2 ± 0.2	96
		(W)	0.9 ± 0.4	76.4 ± 1.9	4
TAW3	Ti-40.0Al-1.5 W[b]	(αTi)	42.3 ± 0.2	0.9 ± 0.1	21
		(βTi, W)	40.4 ± 0.3	1.7 ± 0.1	79
TAW4	Ti-40.6Al-1.8 W[b]	(αTi)	42.4 ± 0.2	1.1 ± 0.1	25
		(βTi, W)	40.0 ± 0.2	2.2 ± 0.1	75
TAW5	Ti-44.5Al-1.1 W[b]	(αTi)	43.3 ± 0.6	1.1 ± 0.1	76
		(βTi, W)	[c]	[c]	< 1
		TiAl	48.4 ± 0.5	0.9 ± 0.2	24
TAW6	Ti-44.8Al-0.9 W[b]	(αTi)	43.0 ± 0.3	0.8 ± 0.1	71
		TiAl	49.5 ± 0.5	0.5 ± 0.1	29
TAW7	Ti-47.1Al-4.1 W[b]	(βTi, W)	40.8 ± 0.3	7.4 ± 0.1	33
		TiAl	50.0 ± 0.2	1.6 ± 0.1	67
TAW8	Ti-51.3Al-3.2 W	TiAl	52.1 ± 0.3	2.0 ± 0.1	n.d.
		(W)	[c]	[c]	n.d.
TAW9	Ti-50.8Al-6.6 W	TiAl	54.0 ± 1.2	2.2 ± 0.1	n.d.
		(W)	[c]	[c]	n.d.
TAW10	Ti-56.0Al-3.6 W	TiAl	57.4 ± 0.5	2.3 ± 0.1	n.d.
		(W)	[c]	[c]	n.d.

[a] Different composition compared to the as-cast alloy due to macroscopic inhomogeneity.
[b] As-cast composition.
[c] Equilibrium composition could not be measured because the particles were too small.

Table 8
Phases and lattice parameters of selected alloys as obtained by HEXRD measurements (accuracy of the lattice parameters is ± 0.0001 nm).

Alloy No.	Heat treatment temperature (°C)	Phases	Crystal structure type (see also Table 1)	Lattice parameters (nm)	
				a	*c*
TAW4	1000	(βTi, W)	Cubic *A2*	0.3205	
		Ti_3Al	Hexagonal $D0_{19}$	0.5761	0.4637
		TiAl	Tetragonal $L1_0$	0.4020	0.4053
	1100	(βTi, W)	Cubic *A2*	0.3206	
		Ti_3Al	Hexagonal $D0_{19}$	0.5757	0.4636
		TiAl	Tetragonal $L1_0$	0.4019	0.4052
	1200	(βTi, W)	Cubic *A2*	0.3204	
		Ti_3Al[b]	Hexagonal $D0_{19}$	0.5750	0.4623
		TiAl	Tetragonal $L1_0$	0.4014	0.4049
TAW5	1000	(βTi, W)	Cubic *A2*	0.3202	
		Ti_3Al	Hexagonal $D0_{19}$	0.5762	0.4637
		TiAl	Tetragonal $L1_0$	0.4020	0.4054
	1100	(βTi, W)	Cubic *A2*	0.3206	
		Ti_3Al	Hexagonal $D0_{19}$	0.5758	0.4639
		TiAl	Tetragonal $L1_0$	0.4018	0.4053
	1200	(βTi, W)	Cubic *A2*	0.3204	
		Ti_3Al[b]	Hexagonal $D0_{19}$	0.5754	0.4628
		TiAl	Tetragonal $L1_0$	0.4015	0.4053
	1300	Ti_3Al[b]	Hexagonal $D0_{19}$	0.5747	0.4621
		TiAl	Tetragonal $L1_0$	0.4010	0.4055
TAW8	1000	TiAl	Tetragonal $L1_0$	0.3996	0.4073
		(W)	Cubic *A2*	0.3157	
	1000_prolonged[a]	TiAl	Tetragonal $L1_0$	0.3997	0.4076
		(W)	Cubic *A2*	0.3156	
	1100	TiAl	Tetragonal $L1_0$	0.3996	0.4071
		(W)	Cubic *A2*	0.3157	
	1200	TiAl	Tetragonal $L1_0$	0.3998	0.4067
		(W)	Cubic *A2*	0.3155	
	1300	TiAl	Tetragonal $L1_0$	0.3998	0.4064
		(W)	Cubic *A2*	0.3156	
TAW10	1200	TiAl	Tetragonal $L1_0$	0.3984	0.4074
		(W)	Cubic *A2*	0.3156	

[a] increased heat treatment time from 650 to 1300 h
[b] Equilibrium phase at heat treatment temperature is (αTi), but has transformed to Ti_3Al during cooling. As the HEXRD measurements were performed at room temperature, the lattice parameters of (αTi) could not be determined and instead those of Ti_3Al were obtained.

transformation temperature, Ti_3Al + (βTi,W) + TiAl are the equilibrium phases (see Fig. 5c and Table 8).

Alloy TAW7 (Ti-47.1Al-4.1 W) was heat-treated at 1200 and 1300 °C resulting in a two-phase microstructure composed of (βTi,W) and TiAl (Fig. 6a). The three alloys with Al content greater than 50 at% Al (TAW8, TAW9, and TAW10) exhibit a microstructure consisting of a TiAl matrix and grayish appearing (in BSE contrast), primary crystallized dendritic-shaped regions with very fine-scaled, W-rich (bright BSE contrast) precipitates (Fig. 6b-d). These fine precipitates are too small to be measured with EPMA (minimum spot size is 1 μm). In order to check whether additional heat treatment times lead to a growth of the particles that allows measurement of the phase compositions, pieces cut from the already heat-treated alloys TAW8 and TAW10 were subjected to additional heat treatments at 1000, 1100, 1200, and 1300 °C, doubling the original times (to 1300, 800, 60, and 40 h, respectively). However, no significant change in the microstructure was observed (Fig. 6c,d), and the composition of TiAl was found to remain unchanged (within the experimental error limits). The values for TAW8 and TAW10 listed in Tables 5–7 are the results of the measurements performed after the prolonged heat treatments. Some of these alloys were investigated using TEM and TEM-EDS. These measurements in combination with the results from HEXRD show that the bright precipitates (in BSE contrast) belong to the (W) solid-solution as is discussed below in Section 4.2.

4. Discussion

Based on the experimental results presented above and some additional information from the literature discussed below, partial isothermal sections between 800 and 1300 °C were established (Figs. 7–12). Two alternative versions for the 800 °C isothermal section (Fig. 7) are shown and discussed below in Section 4.1. For the binary boundary systems Ti–Al and Ti–W, the assessed phase diagrams as reported in [19,20] and [22], respectively, were used. It is known from the work of Sparks et al. [14] that there is an equilibrium between the Al-rich phase $TiAl_3$ and the (W) solid solution at 1200 °C. If we assume that this is also true at 1300 °C and for the entire temperature range down to room temperature, this means that there can be no equilibria between the intermetallic phases of the Al-W boundary system and the Ti-rich part of the ternary system, i.e., the Al-W system is of no relevance for the present results (except for the solubility of Al in (W), for which values from ref. [23] were used). Sparks et al. [14] reported a three-phase equilibrium between $TiAl_3$, the (W) solid solution, and a

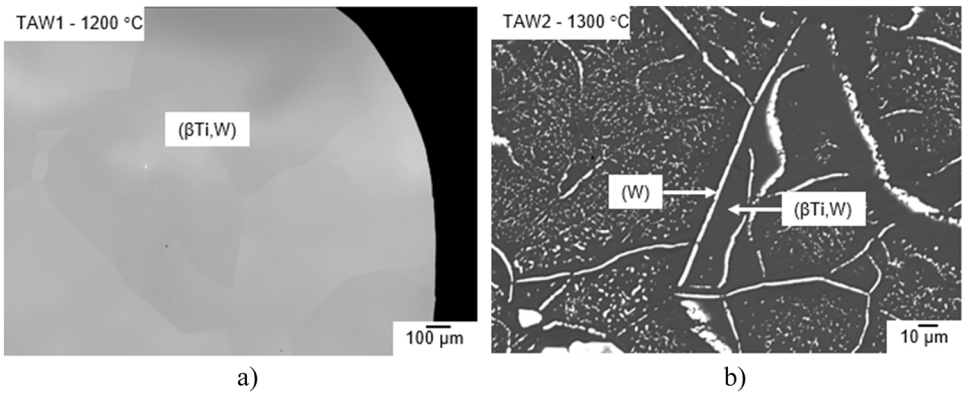

Fig. 2. SEM back-scattered electron (BSE) micrographs of a) alloy TAW1 (Ti-28.3Al-6.1 W) heat-treated at 1200 °C showing a single-phase (βTi,W) microstructure; b) alloy TAW2 (Ti-28.8Al-13.1 W) heat-treated at 1300 °C showing a two-phase microstructure consisting of (βTi,W) and (W).

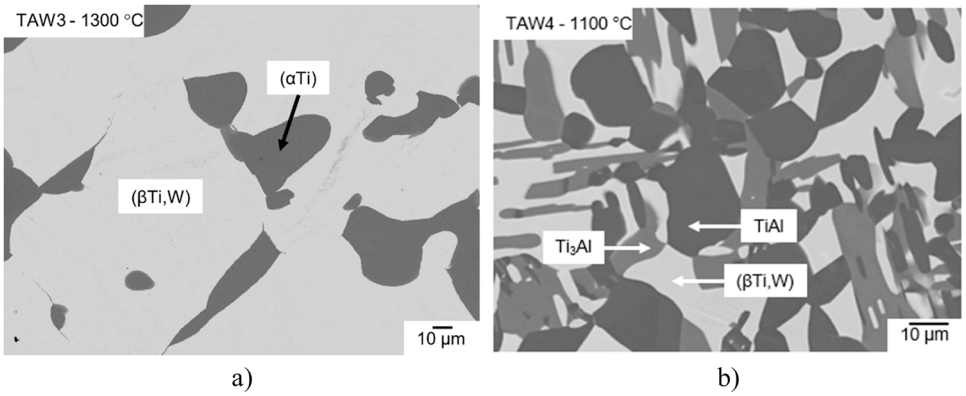

Fig. 3. SEM micrographs (BSE mode) of a) alloy TAW3 (Ti-40.0Al-1.5 W) heat-treated at 1300 °C showing a two-phase microstructure (αTi) (dark) + (βTi,W) (bright); b) alloy TAW4 (Ti-40.6Al-1.8 W), heat-treated at 1100 °C showing a three-phase microstructure composed of (βTi,W) (bright), Ti_3Al (gray), and TiAl (dark).

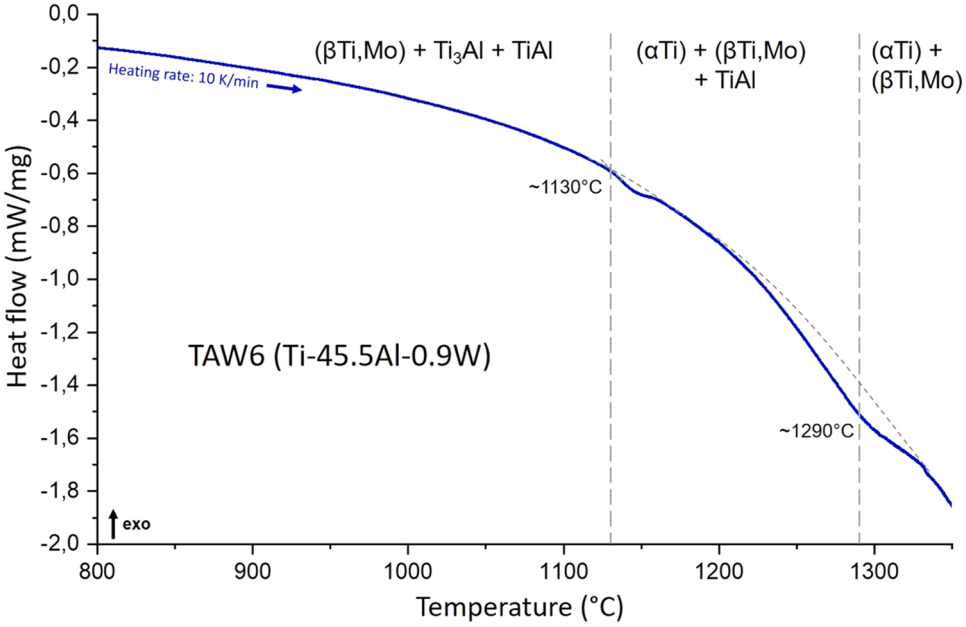

Fig. 4. DTA heating curve of the as-cast state of alloy TAW6 (Ti-45.5Al-0.9 W) showing the transition from Ti_3Al to (αTi) at ~ 1130 °C and the completion of the dissolution of TiAl at ~1290 °C.

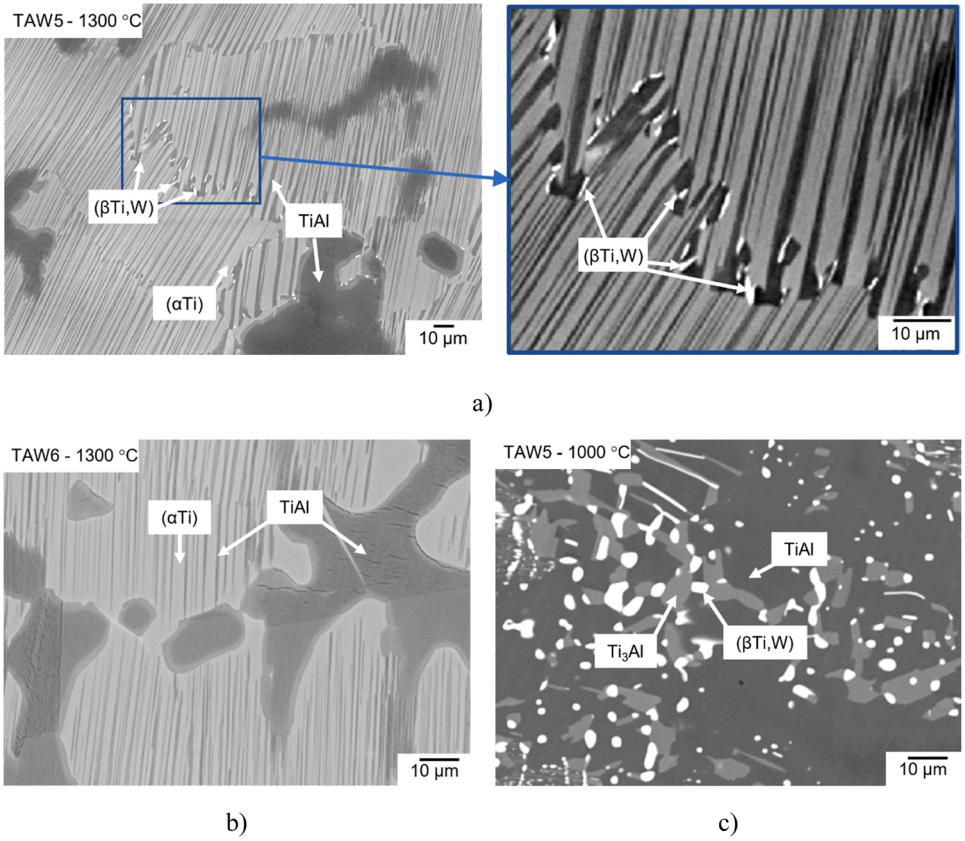

Fig. 5. SEM micrographs (BSE mode) of a) alloy TAW5 (Ti-45.0Al-1.1 W) and b) alloy TAW6 (Ti-45.5Al-0.9 W) after heat treatment at 1300 °C. The microstructure consists of the TiAl matrix (dark regions) and extended lamellar (αTi) + TiAl regions. The microstructure of the slightly W-richer alloy TAW5 contains a small amount of (βTi,W) particles along the boundaries of the lamellar colonies (well visible as bright particles in the enlarged image section on the right side). (The gray contrast at the edges of the dark TiAl regions results from an imperfect sample preparation; measurements of the chemical composition show that it is the same as in the interior of these dark regions). The BSE micrograph in c) of alloy TAW5 (Ti-45.0Al-1.1 W) after heat treatment at 1000 °C shows the three-phase equilibrium (βTi,W) + Ti_3Al + TiAl.

third phase with approximate composition Ti-68Al-4 W, which is outside the compositional range studied here. The W-rich end of the respective three-phase triangle is included in the present isothermal sections. Since the composition value of the (W) solid solution was not given by Sparks et al., the exact position of this partial triangle is not clear, which is why it is shown here only by thin, dash-dotted, gray lines.

Most of the tie lines between TiAl and the (W) solid solution are drawn as dashed lines because the exact composition of the fine (W) particles with diameters < 1 µm could not be measured. Even if the (W) composition values are not known, the direction of the tie lines can be determined from the available measurements by plotting a series of mixed analysis points (i.e., fine white particles with surrounding gray phase) as exemplified in Fig. 13. For an explanation why these fine particles indeed are the (W) solid solution, see Section 4.2.

In the Ti–W system, a miscibility gap exists in the (βTi,W) phase field below 1250 °C. This miscibility gap extends into the ternary system, where it leads to a large (βTi,W) + (W) two-phase field even at 1300 °C (see Fig. 12).

In the following Sections 4.1 and 4.2, the solubility of the ternary elements in the binary boundary phases and the phase equilibria between TiAl and the (W) solid-solution are discussed.

4.1. Solubility of ternary elements in the boundary phases (αTi), (βTi,W), Ti_3Al, TiAl, and (W), and phase equilibria at 800 °C

(αTi): In the binary Ti-Al system, the (αTi) phase is split into a Ti-rich and an Al-rich phase field, which are stable below 1170 °C and between 1120 and 1491 °C, respectively [19,20]. The solubility of W in the latter, Al-rich (αTi) phase at 1200 (Fig. 11) and 1300 °C (Fig. 12) is determined by the composition of (αTi) in the tie-triangle (αTi) + (βTi,W) + TiAl. The solubility values obtained from the present experiments are 1.0 at% W at 1200 °C and 1.1 at% W at 1300 °C. A similar value of 1.1 at% W was measured by Kainuma et al. [16] for 1200 °C, while they reported an increased solubility of 2.4 at% for 1300 °C [16]. The solubility of W in the Ti-rich (αTi) phase was not determined in the present study. The only values published in the literature are those of Oleynikova et al. [13], who report a solubility of "about 1 wt%" (0.4 at%) at 1000 and 800 °C.

(βTi,W): The Al solubility in (βTi,W) at 1300 °C lies close to the Al content of the (βTi,W) phase in alloy TAW7 (40.8 at%) and is estimated to be about 41 at%. This is consistent with the results of Kainuma et al. [16] and Hashimoto et al. [15], who report values of about 40 at% Al. With decreasing temperature, this value slightly drops reaching about 36 at% at 1000 °C (Figs. 9–11), which again is consistent with the results of Kainuma et al. [16]. These solubility values, however, do not agree with the results of Oleynikova et al. [13], who reported a maximum solubility of 17.1 at% Al at 1100 °C. Additionally, they found phase equilibria other than those presented here, which might be a result of the strong carbon contamination of their samples [13]. Based on the consistency between the here presented results and the above mentioned results of Kainuma et al. [16] and Hashimoto et al. [15,18] in the temperature range above 1000 °C, the experimental observations of Oleynikova et al. [13] are not considered in this range. At 800 °C Oleynikova et al. [13] report a solubility of only ~3 at% Al in (βTi,W) and also found (αTi), (βTi,W) and (W) to be in equilibrium. This strong decrease of Al solubility compared to 1000 °C is theoretically only possible if two transition-type reactions (βTi,W) + TiAl = Ti_3Al + (W) and (βTi,W) + Ti_3Al = (αTi) + (W) take place. The version of the 800 °C isothermal section in Fig. 7b is based on this assumption. If these transition-type reactions are not taking place, a much higher Al solubility in (βTi,W) would be expected. A tentative isothermal section of this case is shown in Fig. 7a. At 800 °C the morphology of the microstructure is very fine-scaled in alloy TAW4. Unfortunately, the microstructure constituents are too small to be measured by EPMA. Therefore, the composition cannot be measured and identification of the W-rich phase cannot be made based on the composition. As the DTA

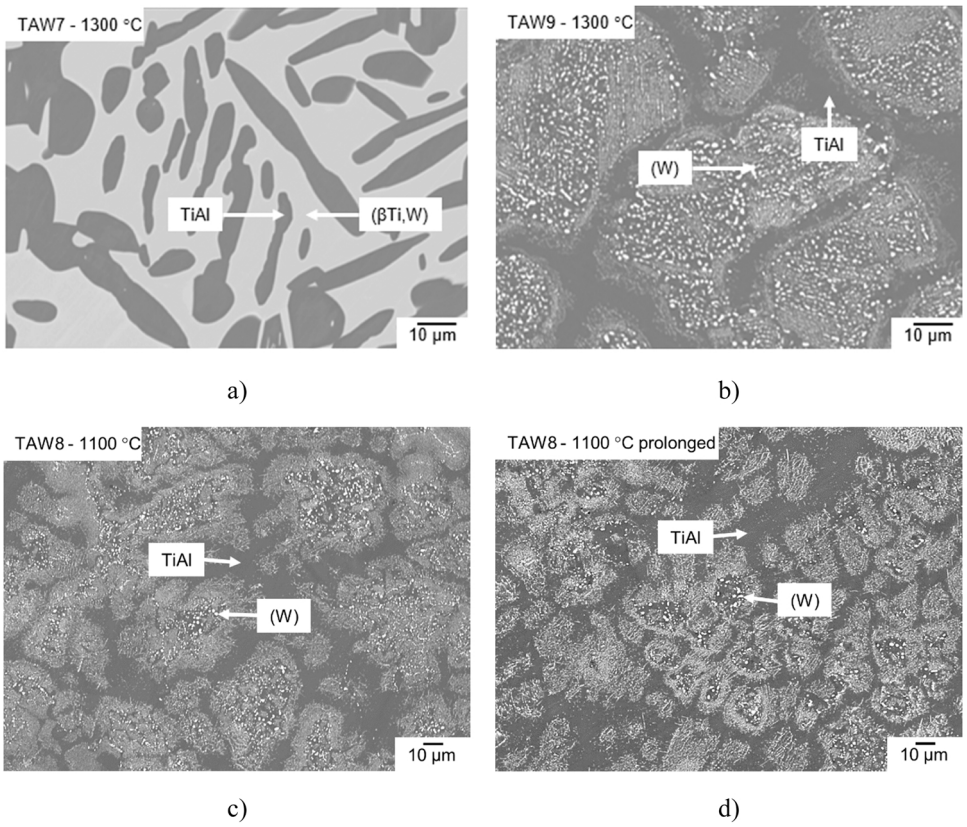

Fig. 6. SEM micrographs (BSE mode) of a) alloy TAW7 (Ti-47.1Al-4.1 W) heat-treated at 1300 °C showing a two-phase microstructure (βTi,W) (bright) + TiAl (dark), b) alloy TAW9 (Ti-50.8Al-6.6 W) heat-treated at 1300 °C showing a TiAl matrix with bright (W) precipitates, and c,d) alloy TAW8 (Ti-50.2Al-3.0 W) heat-treated at 1100 °C for 400 and 800 h, respectively, showing the same microstructure constituents as in b).

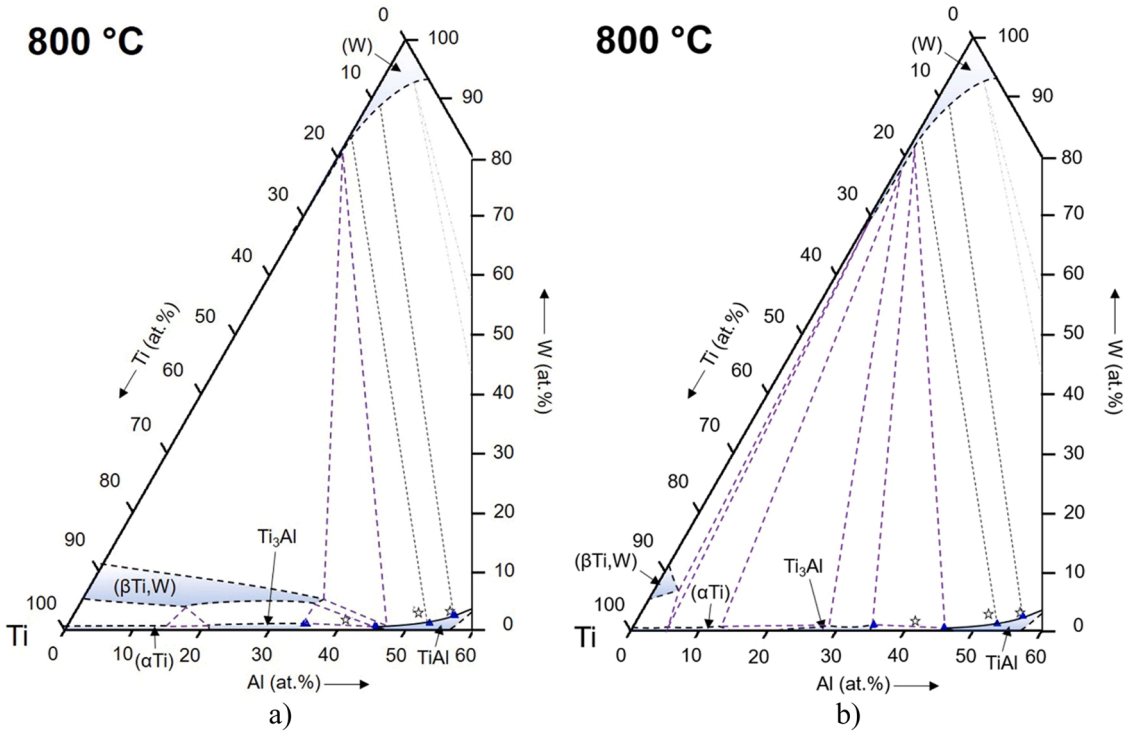

Fig. 7. Two tentative versions of a partial isothermal section of the Ti–Al–W system at 800 °C based on the experimental results tabulated in Table 4 and a) the here presented isothermal sections at higher temperatures or b) assuming a solubility of only 3 at% Al in the (βTi,W) phase as indicated by the data of Oleynikova et al. [13]. The as-cast compositions of the samples are represented by the gray stars, the purple lines mark the three-phase equilibria, and blue symbols and black lines mark the phase compositions, tie lines, and resulting phase boundaries.

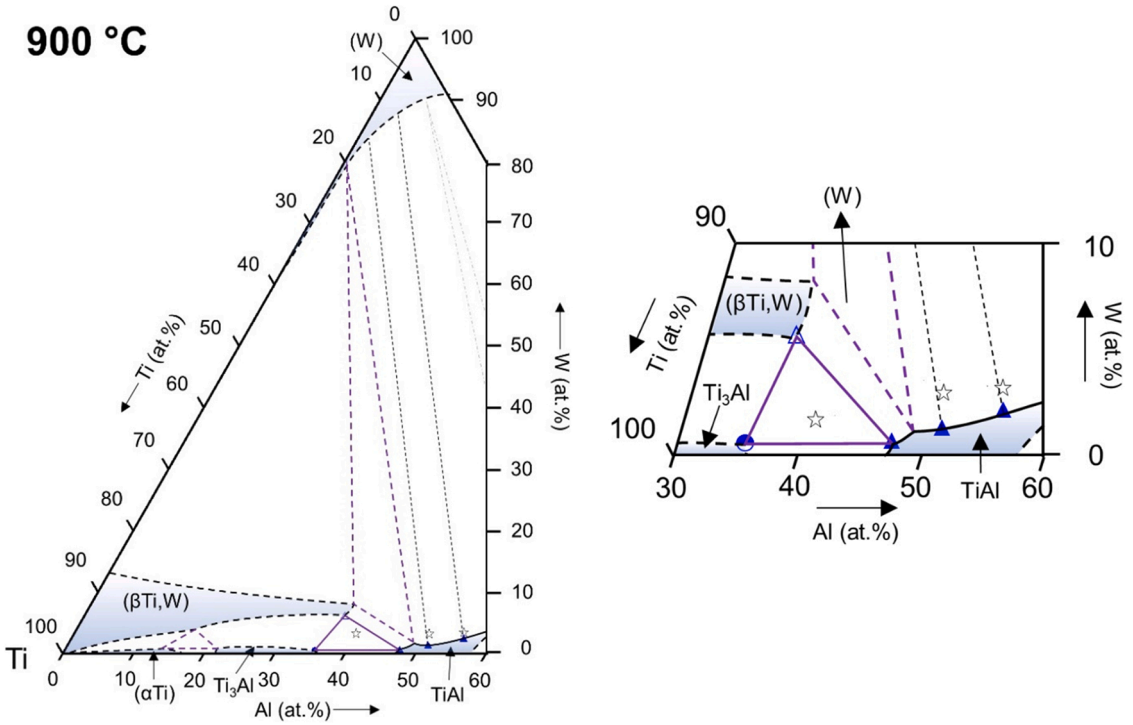

Fig. 8. Partial isothermal section of the Ti–Al–W system at 900 °C based on the experimental results tabulated in Table 4. A magnification of the region between 30 and 60 at% Al and 0–10 at% W is shown on the right. The stars indicate the overall compositions of the samples, and the blue symbols mark the measured phase compositions (empty triangles: (βTi,W), filled triangles: TiAl, half-filled circles: Ti_3Al).

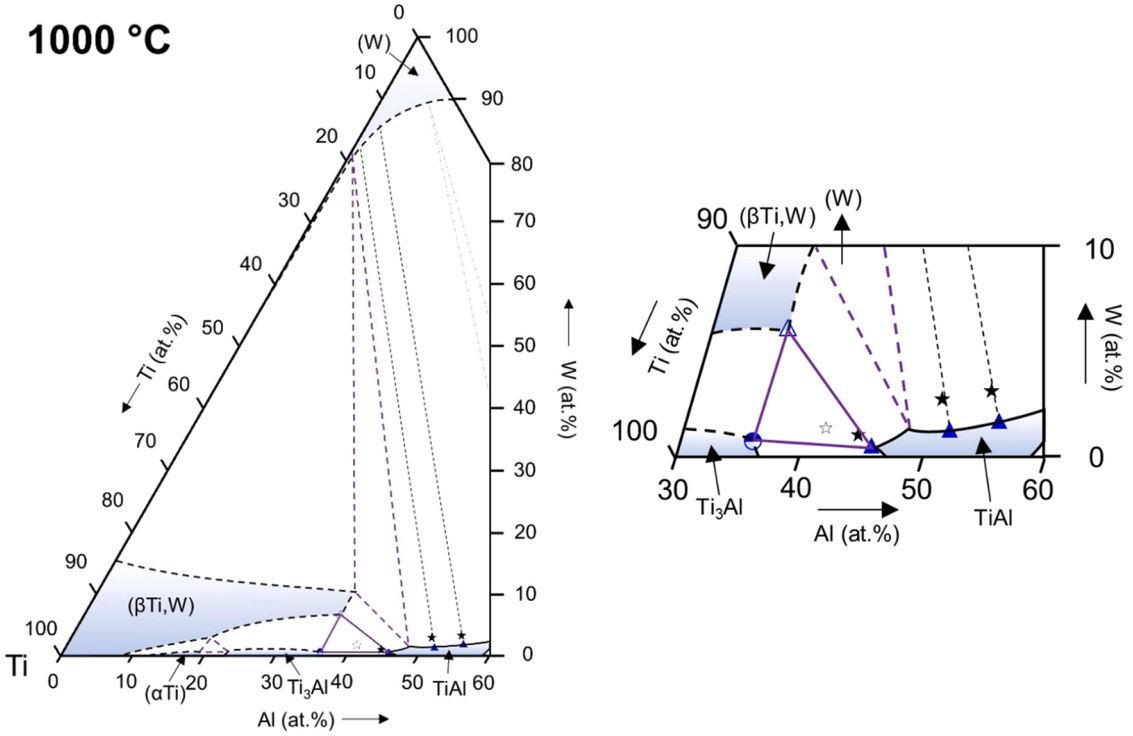

Fig. 9. Partial isothermal section of the Ti–Al–W system at 1000 °C based on the experimental results tabulated in Table 5. A magnification of the region between 30 and 60 at% Al and 0–10 at% W is shown on the right. The stars indicate the overall compositions of the samples (empty stars: as cast composition, black stars: after heat treatment at 1000 °C). The blue symbols mark the measured phase compositions (empty triangles: (βTi,W), filled triangles: TiAl, half-filled circles: Ti_3Al).

measurements show no thermal effect that could be associated with a transition-type reaction in this temperature range, it might be assumed that Ti_3Al, TiAl, and (βTi,W) are in equilibrium at 800 °C (Fig. 7a), as is also the case between 900 and 1100 °C (Figs. 8–10). Nevertheless, the absence of the thermal effect may be due to the slow diffusion of W in this temperature range, which is evident from the fine-scaled

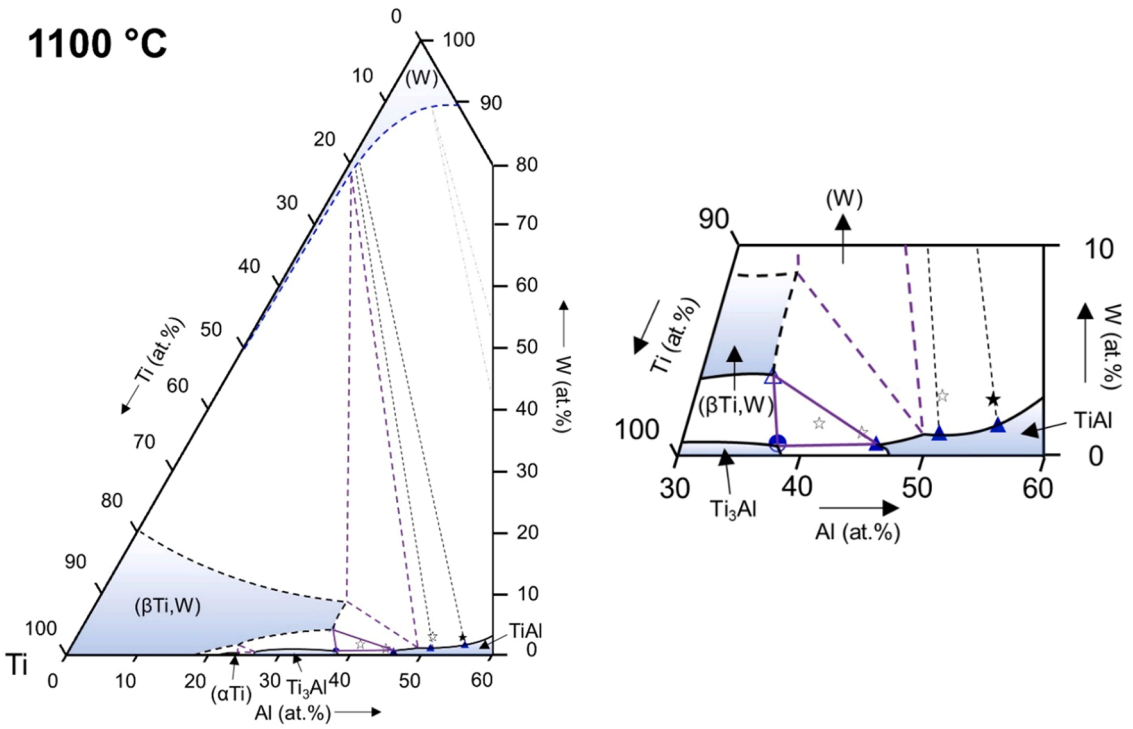

Fig. 10. Partial isothermal section of the Ti–Al–W system at 1100 °C based on the experimental results tabulated in Table 5. A magnification of the region between 30 and 60 at% Al and 0–10 at% W is shown on the right. The stars indicate the overall compositions of the samples (empty stars: as cast composition, black stars: after heat treatment at 1100 °C). The blue symbols mark the measured phase compositions (empty triangles: (βTi,W), filled triangles: TiAl, half-filled circles: Ti_3Al).

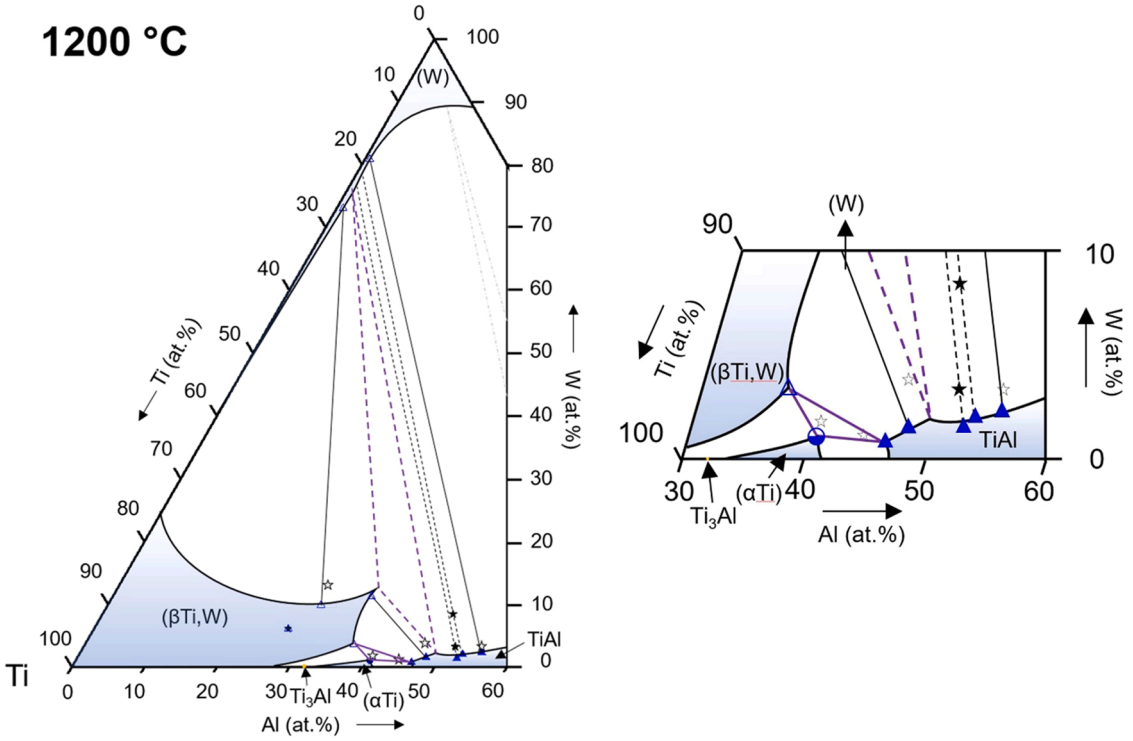

Fig. 11. Partial isothermal section of the Ti–Al–W system at 1200 °C based on the experimental results tabulated in Table 6. A magnification of the region between 30 and 60 at% Al and 0–10 at% W is shown on the right. The stars indicate the overall compositions of the samples (empty stars: as cast composition, black stars: after heat treatment at 1200 °C). The blue symbols mark the measured phase compositions (empty triangles: (βTi,W) and (W), filled triangles: TiAl, half-filled circles: (αTi)).

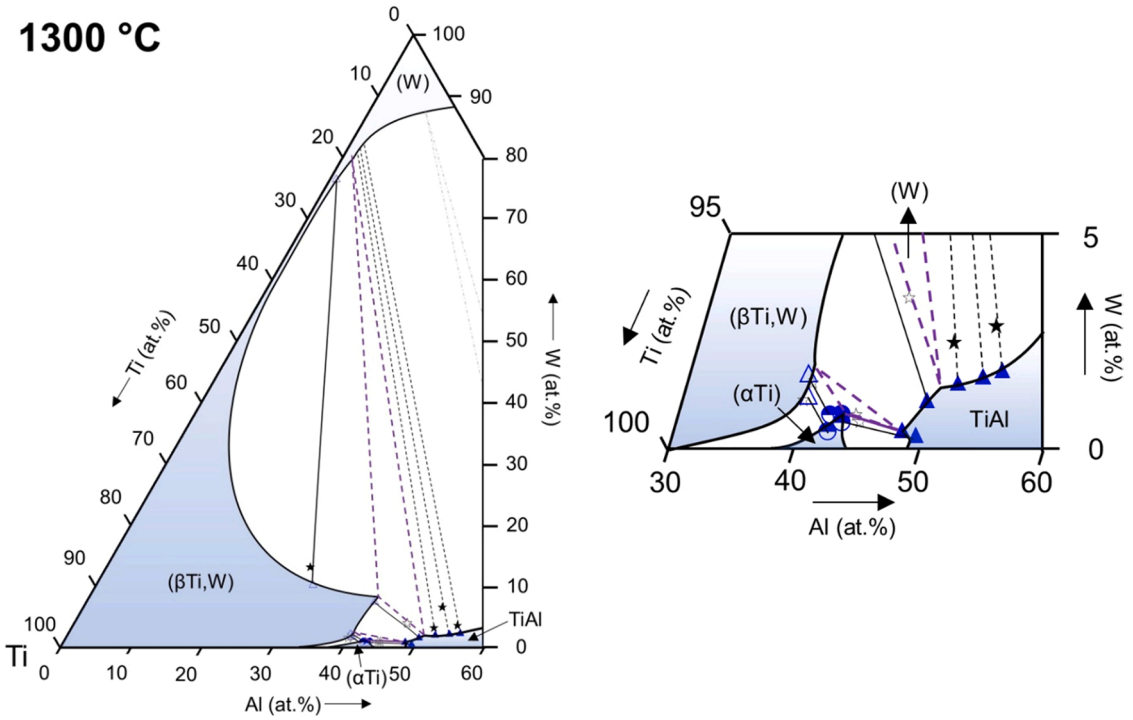

Fig. 12. Partial isothermal section of the Ti–Al–W system at 1300 °C based on the experimental results tabulated in Table 7. A magnification of the region between 30 and 60 at% Al and 0–5 at% W is shown on the right. The stars indicate the overall compositions of the samples (empty stars: as cast composition, black stars: after heat treatment at 1300 °C). The blue symbols mark the measured phase compositions (empty triangles: (βTi,W) and (W), filled triangles: TiAl, half-filled circles: (αTi)).

microstructure constituents and could mask or even completely prevent the occurrence of the transition-type reactions. Since our experiments do not provide clear evidence whether (βTi,W) or (W) is in equilibrium with Ti_3Al and TiAl, the two versions of the isothermal sections are shown in Fig. 7. To determine the correct phase equilibria and solubility of Al in (βTi,W) at 800 °C, further experiments are necessary.

Ti_3Al: The solubility of W in Ti_3Al is very low and increases slightly with temperature from 0.5 at% at 900 °C to 0.7 at 1100 °C (Tables 4 and 5). Kainuma et al. [16] report a solubility of 0.7 at% W in Ti_3Al at 1000 °C, and Hashimoto et al. [18] also find that the solubility is below 1 at%, which agrees with our results.

TiAl: There are no reports in the literature on the maximum W solubility in TiAl, and this value can also not be determined with the alloys studied here. However, alloys TAW4, 8, and 10 show an increase in W solubility with increasing temperature and Al content of the alloy (see Fig. 14a), which has also been observed in the literature [16].

Additionally, a continuous increase of the *c/a* ratio of TiAl (measured by HEXRD (Table 8)) as function of the Al content of TiAl is observed between 46 and 54 at% Al (Fig. 14b). This corresponds to an increase of the tetragonality of the nearly cubic unit cell with increasing Al content. Similar observations were made in binary TiAl alloys, where a continuous increase is observed in this composition range as well [26,34,35]. At higher Al contents, the *c/a* ratio appears to reach a maximum at about 58 at% [26] and decreases again at Al contents above 60 at% [26,36]. The addition of W appears to have no or an only negligible effect on the lattice parameters and the *c/a* ratio of the TiAl phase. Similar weak effects of W on the lattice parameters are found for Ti_3Al, which can probably be attributed to the similar atomic sizes of Ti and W.

(W): The Al contents found in the (W) solid solution of the present alloys are low (< 1 at% at 1200 and 1300 °C in alloys TAW2 and 10, see Tables 6 and 7). In the binary Al–W boundary system, they are significantly higher reaching about 11 at% at 1300 °C and decreasing to about 7 at% at 800 °C [23]. The phase boundary of the (W) phase field in the isothermal sections in Figs. 7–12 is tentatively drawn based on this information and assuming that the Al content decreases with decreasing temperature.

4.2. Phase equilibria with the (W) solid solution

The heat-treated alloys TAW8, 9, and 10 show a microstructure consisting mainly of TiAl and very fine precipitates (see Figs. 6b-d and 15a as examples). As already mentioned in Section 3, these precipitates have a cubic crystal structure according to HEXRD, but they are too small to determine their composition by EPMA even after doubling the heat treatment times. This leaves open several possibilities as to which phase the precipitates belong to: i) the (βTi,W) phase; ii) the tungsten solid-solution (W); or iii) a hitherto unknown, ternary intermetallic compound with cubic crystal structure. As will be explained in the following, the present HEXRD and TEM investigations prove that the second possibility is true:

Both (W) and (βTi,W) have a bcc lattice with similar lattice parameters. Pure W has a lattice parameter of $a = 0.3165$ nm [37] and that of pure βTi is $a = 0.3307$ nm at 900 °C [37], which corresponds to an approximated room temperature value of about $a = 0.328$ nm (as pure βTi cannot be quenched, a direct measurement of the room temperature lattice parameter is not possible; however, this value can be estimated from the high-temperature values using an approximate average coefficient of thermal expansion of 10×10^{-6} [38,39]). In the binary Ti-Al and ternary Ti-Al-X systems, large amounts of Al in the range of up to 40 at% can be dissolved in the (βTi) solid solution, resulting in a slight reduction of the pure-Ti lattice parameter (0.328 nm) to values of, e.g., $a = 0.3217$ nm for Ti-Al-Nb [32] and 0.3210 nm for the TNM (Ti-43Al-4 Nb-1Mo-0.08B) alloy. The values measured here for the bcc phases (Table 8) divide into two groups. In the case of the alloys TAW4 and 5, the lattice parameters all lie with only slight deviation around a mean value of 0.3205 nm, and in the case of the W- and Al-richer alloys TAW8 and 10, also with only very slight scatter, there is a mean value of 0.3156 nm. The first value is very similar to the above cited, typical

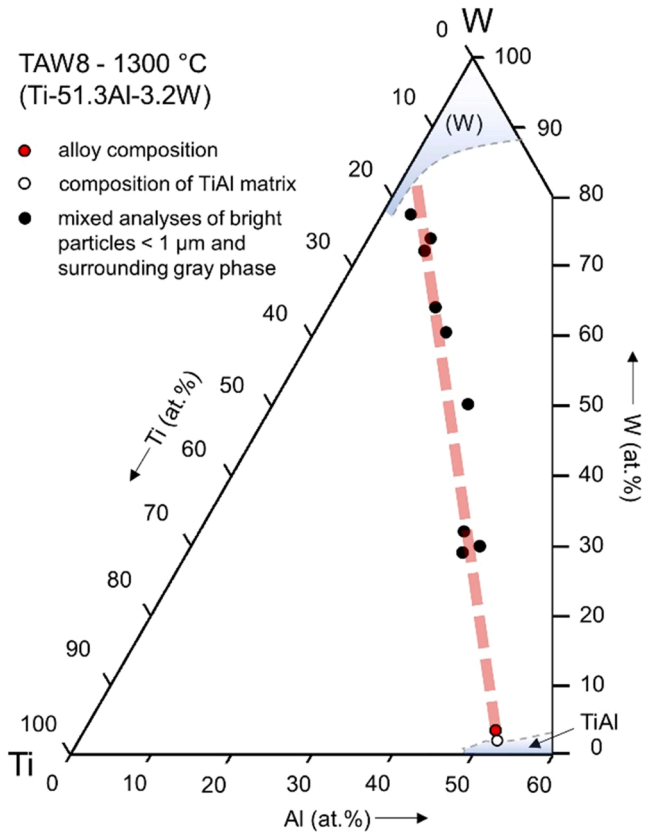

Fig. 13. Example of EPMA values obtained from measurements of fine bright particles with a more or less large proportion of the surrounding gray phase (black circles) in alloy TAW8–1300 °C revealing the direction of the tie line between TiAl and (W). The composition value of the TiAl phase (white circle) is averaged from 15 measured values.

values for the (βTi) solid solution, which perfectly well agrees with the findings from EPMA (see Tables 4–7) for these alloys. The second group of values (centered around 0.3156 nm) obtained in alloys TAW8 and 10 is very close to that of pure W (0.3165 nm), which is why we attribute this bcc phase to the (W) solid solution.

This conclusion is finally confirmed by TEM and TEM-EDS analyses of the fine precipitates. Fig. 15a shows an SEM-BSE micrograph of alloy TAW10 heat-treated at 1200 °C. A more detailed view of the microstructure in a typical region with a high density of precipitates was obtained by TEM investigations of this sample. Fig. 15b and c show a respective bright-field (BF) and a high-angle annular dark-field (HAADF) image, and Fig. 15d is a TEM-EDS mapping ($W_{M\alpha}$-line) of the region in Fig. 15c. These images reveal that the microstructure consists only of the TiAl matrix phase and the fine precipitates, i.e., the grayish appearing background in the SEM micrograph of this sample results from the fine mixture of these two phases. Some isolated precipitates were found along the edges of a hole in the TEM sample (see Fig. 15c), which allowed their composition to be measured without the influence of the TiAl matrix (Fig. 15c,d). In addition, selected area electron diffraction experiments were performed, which confirm the body-centered cubic crystal structure of the precipitates. From their measured composition (Ti-0.7Al-80.8 W), it is concluded that these precipitates are indeed the (W) solid solution. This also means that there is no ternary intermetallic compound in the composition range studied.

Since the alloys are produced from the pure metals Ti, Al, and W, it could be assumed that the fine (W) precipitates actually originate from W particles that did not completely dissolve in the synthesis process. This, however, is not true as is obvious from inspecting the microstructure of the as-cast alloys. Fig. 16a shows a micrograph of the as-cast state of alloy TAW10 consisting of the TiAl matrix and primary crystallized, metastable (βTi,W) phase (with a composition of Ti-52.3Al-3.7 W). There is not any indication of the fine W particles, which are characteristic for all heat-treated states (cf. Fig. 16b for the 900 °C and Fig. 15a for the 1200 °C heat-treated states). Obviously, the primary (βTi,W) dendrites decompose during the heat treatments into the above described fine mixture of the equilibrium phases TiAl + (W) and, as the diffusion of W seems to be very slow, the growth of the fine particles needs long times.

The observation of the three two-phase equilibria (βTi,W) + TiAl (alloy TAW7 quenched from 1200 (Fig. 11) and 1300 °C (Fig. 6a and Fig. 12)), (βTi,W) + (W) (alloy TAW2 at 1200 (Fig. 11) and 1300 °C (Fig. 2b and Fig. 12)), and TiAl + (W) (alloys TAW8–10 as described above) proves the existence of the three-phase equilibrium (βTi,W) + TiAl + (W), and also the position of the respective three-phase field is well defined (at least at 1200 and 1300 °C) by these experimental tie lines.

5. Conclusions

Six partial isothermal sections of the ternary Ti-Al-W system between

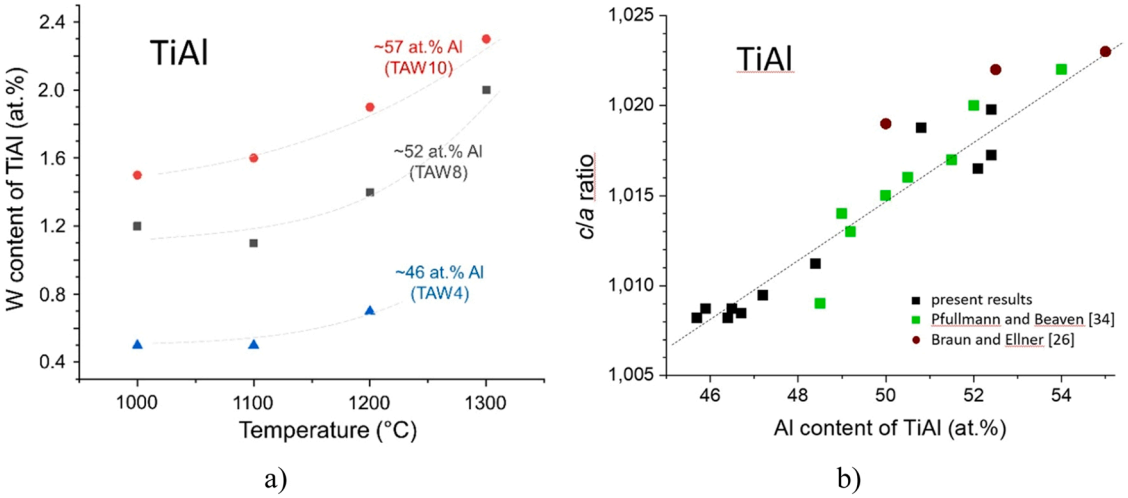

Fig. 14. a) Increase of the W content in the TiAl phase as a function of temperature for the alloys TAW4 (TiAl with ~46 at% Al), TAW8 (TiAl with ~52 at% Al), and TAW10 (TiAl with ~57 at% Al) in the temperature range from 1000° to 1300°C; b) c/a lattice parameter ratios of W-containing TiAl (black squares) from HEXRD results (s. Table 8) compared with values from the literature for binary TiAl alloys showing a continuous increase with increasing Al content of TiAl.

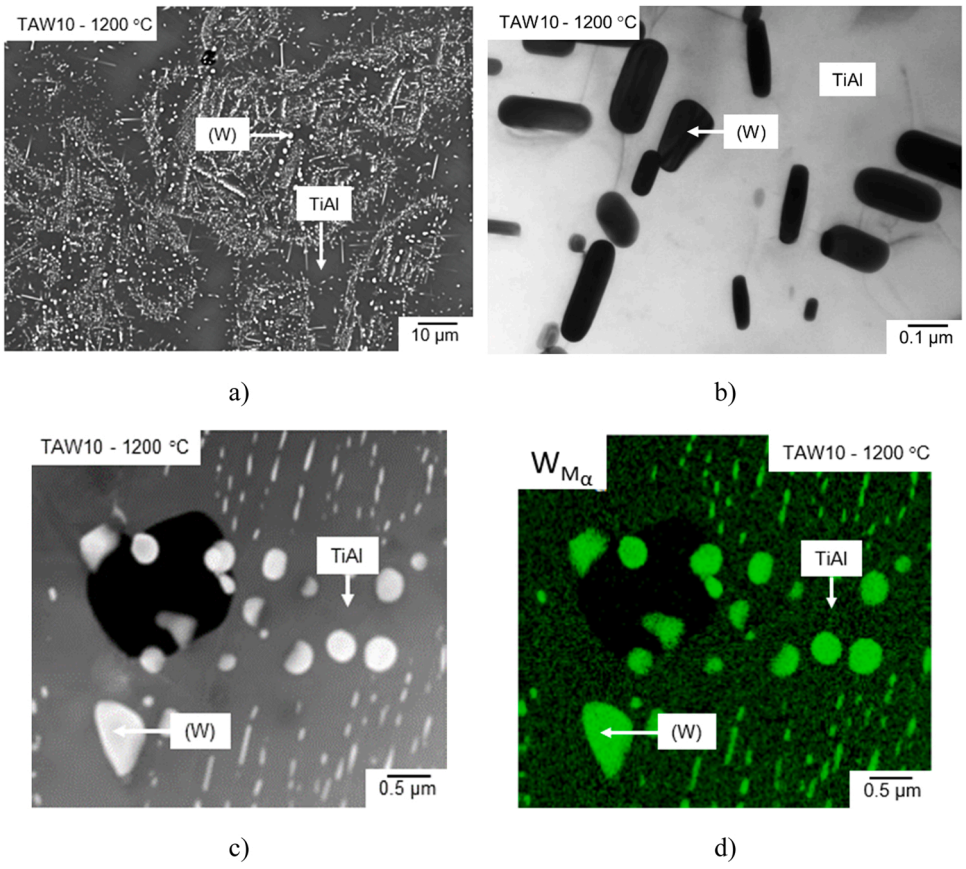

Fig. 15. a) SEM micrograph (BSE mode) of alloy TAW10 (Ti-54.9Al-3.3 W) heat-treated at 1200 °C showing a TiAl matrix with bright (W) precipitates; b) bright-field TEM image of the gray/bright area; c) respective HAADF image and d) TEM-EDS map using the $W_{M\alpha}$ line showing that the bright precipitates are rich in W and that only two phases are present.

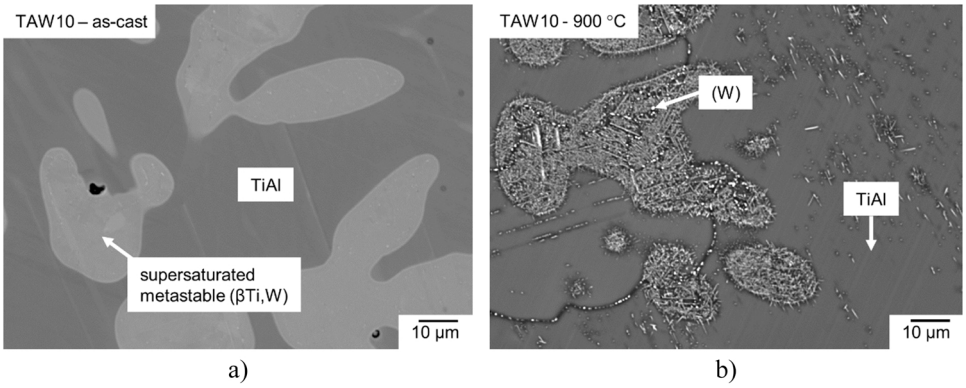

Fig. 16. Comparison of as-cast and heat-treated microstructure of alloy TAW10 (SEM micrographs in BSE mode): a) as-cast state, showing TiAl and primary solidified, supersaturated metastable (βTi,W) solid solution containing 52.3 at% Al and 3.7 at% W, and b) after heat treatment at 900 °C, revealing the decomposition of the former metastable regions into TiAl and very fine (W) particles (white).

800 and 1300 °C have been established covering a composition range from 0 to 60 at% Al and 0–100 at% W. For this purpose, ten ternary alloys were synthesized, heat-treated at different temperatures, and analysed by a combination of SEM, EPMA, HEXRD, DTA, and TEM results. The diffusion of W in the ternary alloys is very slow, which is apparent from the small size of the precipitates observed in some alloys despite the long heat treatment times of up to 2000 h, and by the only slight differences between the microstructures of the as-cast and heat-treated alloys in some cases (e.g. TAW8 and TAW10 at 800 and 900 °C).

No ternary intermetallic phase was detected, and no experimental evidence for *B*2-ordering of the (βTi,W) solid solution was found. The miscibility gap between the Ti-rich (βTi,W) and the W-rich (W) solid solutions, which exists in the binary Ti–W system below 1250 °C, extends into the ternary system up to at least 1300 °C, where a two-phase equilibrium (βTi,W) + (W) was observed in the present investigations.

TEM and TEM-EDS investigations confirm the existence of phase equilibria between TiAl and the (W) solid solution. As the Al contents in the (W) solid solution at 1200 and 1300 °C are very low (< 1 at%), the two-phase field TiAl + (W) extends almost completely through the ternary composition triangle.

The solubility of W in the phases (αTi) and Ti_3Al is below ~1 at% at all temperatures. Higher W contents of up to 2.3 at% were found in the

TiAl phase. From the alloys studied here, the determination of the solubility limit of W in TiAl was not possible.

The Al solubility in (βTi,W) reaches more than 40 at% at high temperatures (41 at% at 1300 °C) and only slightly decreases down to 35 at % at 1000 °C. According to Oleynikova et al. [13], the maximum Al content in (βTi,W) strongly reduces to only about 4 at% at 800 °C. This would require two transition-type reactions (βTi,W) + TiAl -> Ti_3Al + (W) and (βTi,W) + Ti_3Al -> (αTi) + (W) to occur. However, from the present experimental results there is no evidence for these reactions and a respective strong decrease in solubility. In order to solve this problem, further alloys with significantly longer heat treatment times will have to be investigated in the future.

CRediT authorship contribution statement

Benedikt Distl: Conceptualization, Methodology, Formal analysis, Investigation, Writing – original draft, Visualization. **Boryana Rashkova:** Methodology, Investigation. **Frank Stein:** Conceptualization, Methodology, Writing – review & editing, Supervision, Funding acquisition.

Declaration of Competing Interest

The authors declare that they have no known competing financial interests or personal relationships that could have appeared to influence the work reported in this paper.

Data Availability

Data will be made available on request.

Acknowledgement

The authors gratefully acknowledge funding from the Clean Sky 2 Joint Undertaking under the European Union's Horizon 2020 research and innovation program under grant agreement No. 820647. The authors also thank Dr. Katja Hauschildt and Prof. Florian Pyczak, from Helmholtz-Zentrum Hereon for the HEXRD measurements.

Prime novelty statement

The authors confirm the novelty of the research which is apparent by the few manuscripts published in this ternary system since the 1970 s „The manuscript has not been published before and is also not under consideration for publication anywhere else.

References

[1] D.E. Larsen, Status of investment cast gamma titanium aluminides in the USA, Mater. Sci. Eng. A 213 (1) (1996) 128–133, https://doi.org/10.1016/0921-5093(96)10234-3.
[2] S. Naka, M. Thomas, C. Sanchez, T. Khan, Development of third generation castable gamma titanium aluminides: role of solidification paths, in: M.V. Nathal, R. Darolia, C.T. Liu, P.L. Martin, D.B. Miracle, R. Wagner, M. Yamaguchi (Eds.), Proc. 2nd International Symposium Structural Intermetallics, ISSI-2, TMS Warrendale, Warrendale, PA, 1997, pp. 313–322.
[3] M. Grange, J.L. Raviart, M. Thomas, Influence of microstructure on tensile and creep properties of a new castable TiAl-based alloy, Metall. Mater. Trans. A 35 (7) (2004) 2087–2102, https://doi.org/10.1007/s11661-004-0157-x.
[4] H. Jabbar, J.P. Monchoux, M. Thomas, A. Couret, Microstructures and deformation mechanisms of a G4 TiAl alloy produced by spark plasma sintering, Acta Mater. 59 (20) (2011) 7574–7585, https://doi.org/10.1016/j.actamat.2011.09.001.
[5] T. Voisin, J.-P. Monchoux, M. Perrut, A. Couret, Obtaining of a fine near-lamellar microstructure in TiAl alloys by Spark Plasma Sintering, Intermetallics 71 (2016) 88–97, https://doi.org/10.1016/j.intermet.2016.01.003.
[6] A. Couret, T. Voisin, M. Thomas, J.-P. Monchoux, Development of a TiAl alloy by spark plasma sintering, JOM 69 (12) (2017) 2576–2582, https://doi.org/10.1007/s11837-017-2549-6.
[7] A. Couret, J.-P. Monchoux, D. Caillard, On the high creep strength of the W containing IRIS-TiAl alloy at 850 °C, Acta Mater. 181 (2019) 331–341, https://doi.org/10.1016/j.actamat.2019.09.056.
[8] A. Couret, D. Reyes, M. Thomas, N. Ratel-Ramond, C. Deshayes, J.-P. Monchoux, Effect of ageing on the properties of the W-containing IRIS-TiAl alloy, Acta Mater. 199 (2020) 169–180, https://doi.org/10.1016/j.actamat.2020.07.061.
[9] A. Couret, M. Allen, M.W. Rackel, B. Galy, J.-P. Monchoux, V. Güther, F. Pyczak, P. Sallot, M. Thomas, Chemical heterogeneities in tungsten containing TiAl alloys processed by powder metallurgy, Materialia 18 (2021), 101147, https://doi.org/10.1016/j.mtla.2021.101147.
[10] T. Voisin, J.-P. Monchoux, M. Thomas, C. Deshayes, A. Couret, Mechanical properties of the TiAl IRIS alloy, Metall. Mater. Trans. A 47 (12) (2016) 6097–6108, https://doi.org/10.1007/s11661-016-3801-3.
[11] A. Donchev, L. Mengis, A. Couret, S. Mayer, H. Clemens, M. Galetz, Effects of tungsten alloying and fluorination on the oxidation behavior of intermetallic titanium aluminides for aerospace applications, Intermetallics 139 (2021), 107270, https://doi.org/10.1016/j.intermet.2021.107270.
[12] H. Clemens, S. Mayer, Design, processing, microstructure, properties, and applications of advanced intermetallic TiAl alloys, Adv. Eng. Mater. 15 (4) (2013) 191–215, https://doi.org/10.1002/adem.201200231.
[13] S.V. Oleynikova, T.T. Nartova, I.I. Kornilov, The titanium corner of the Ti-Al-W phase diagram, Russ. Met. 1973 (3) (1973) 184–189.
[14] C.J. Sparks, W.D. Porter, J.H. Schneibel, W.C. Oliver, C.G. Golec, Formation of cubic L12 phases from aluminum titanium Al3Ti and aluminum zirconium Al3Zr by transition metal substitutions for aluminum, Mater. Res. Soc. Symp. Proc. 186 (1991) 175–180, https://doi.org/10.1557/PROC-186-175.
[15] K. Hashimoto, M. Kimura, Y. Mizuhara, Alloy design of gamma titanium aluminides based on phase diagrams, Intermetallics 6 (1998) 667–672, https://doi.org/10.1016/S0966-9795(98)00048-X.
[16] R. Kainuma, Y. Fujita, H. Mitsui, K. Ishida, Phase equilibria among α (hcp), β (bcc) and γ (L10) phases in Ti–Al base ternary alloys, Intermetallics 8 (2000) 855–867, https://doi.org/10.1016/S0966-9795(00)00015-7.
[17] K. Hashimoto, H. Hirata, Y. Mizuhara, Phase Stability and High Temperature Tensile Properties of W doped gamma-TiAl, MRS Online Proc. Libr 646 (1) (2000) 546–551, https://doi.org/10.1557/PROC-646-N7.8.1.
[18] K. Hashimoto, High-temperature tensile properties of Ti-Al-X (X=Cr,W) consisting of α2, β and γ in three phases, Mater. Sci. Forum 706- 709 (2012) 1066–1070, https://doi.org/10.4028/www.scientific.net/MSF.706-709.1066.
[19] J.C. Schuster, M. Palm, Reassessment of the binary aluminum-titanium phase diagram, J. Phase Equilibria Diffus. 27 (3) (2006) 255–277, https://doi.org/10.1361/154770306×109809.
[20] M. Palm, Al-Ti Binary Phase Diagram Evaluation, in: G. Effenberg (Ed.), MSI Eureka, MSI, Materials Science International Services GmbH, Stuttgart, 2020, pp. Doc-ID: 20.15634.2.4. https://doi.org/10.7121/msi-eureka-20.15634.2.4.
[21] I. Jung, H. Jang, M. Oh, J. Lee, D. Wee, Microstructure control of TiAl alloys containing β stabilizers by directional solidification, Mater. Sci. Eng. A 329- 331 (2002) 13–18, https://doi.org/10.1016/S0921-5093(01)01494-0.
[22] J.L. Murray, The Ti−W (Titanium-Tungsten) system, Bull. Alloy Ph. Diagr. 2 (2) (1981) 192–196, https://doi.org/10.1007/BF02881477.
[23] P. Wang, W. Xiong, U.R. Kattner, C.E. Campbell, E.A. Lass, O.Y. Kontsevoi, G. B. Olson, Thermodynamic Re-Assessment of the Al-Co-W System, CALPHAD 59 (2017) 112–130, https://doi.org/10.1016/j.calphad.2017.09.007.
[24] T.B. Massalski. Binary Alloy Phase Diagrams, Second ed.,, ASM International, Metals Park, OH, USA, 1990.
[25] J. Braun, M. Ellner, On the partial atomic volume of Aluminium in the Titanium-rich phases of the binary system Ti-Al, Z. für Metallkd. 91 (2000) 389–392.
[26] J. Braun, M. Ellner, B. Predel, Experimental investigations of the structure and stability of the phase TiAl (in German), Z. für Metallkd. 86 (12) (1995) 870–876, https://doi.org/10.1515/ijmr-1995-861212.
[27] T.R.Hogness L.S. T'sai, The diffusion of gases through fused quartz, J. Phys. Chem. 36 (10) (1932) 2595–2600, https://doi.org/10.1021/j150340a007.
[28] R. Kainuma, M. Palm, G. Inden, Solid-phase equilibria in the Ti-rich part of the Ti–Al system, Intermetallics 2 (4) (1994) 321–332, https://doi.org/10.1016/0966-9795(94)90018-3.
[29] B. Distl, K. Hauschildt, F. Pyczak, F. Stein, Phase equilibria in the Ti-rich part of the Ti–Al–Nb system—Part II, High. Temp. Ph. Equilib. 1000 1300 °C J. Ph. Equilib. Diffus. 43 (2022) 554–575, https://doi.org/10.1007/s11669-022-00999-w.
[30] N. Schell, A. King, F. Beckmann, T. Fischer, M. Müller, A. Schreyer, The high energy materials science beamline (HEMS) at PETRA III, Mater. Sci. Forum 772 (2014) 57–61, https://doi.org/10.4028/www.scientific.net/MSF.772.57.
[31] L. Lutterotti, Total pattern fitting for the combined size–strain–stress–texture determination in thin film diffraction, Nucl. Instrum. Methods Phys. Res. B 268 (3) (2010) 334–340, https://doi.org/10.1016/j.nimb.2009.09.053.
[32] B. Distl, K. Hauschildt, B. Rashkova, F. Pyczak, F. Stein, Phase Equilibria in the Ti-Rich Part of the Ti-Al-Nb System—Part I: Low-Temperature Phase Equilibria Between 700 and 900 °C, J. Ph. Equilib. Diffus. 43 (2022) 355–381, https://doi.org/10.1007/s11669-022-00963-8.
[33] B. Distl, A. Walnsch, R.F.L. Mellor, L. Gomell, M. Noori, A. Gedsun, F. Stein, Al-Mo-Ti Ternary Phase Diagram Evaluation, in: A. Watson (Ed.), MSI Eureka, MSI, Materials Science International Services GmbH, Stuttgart, 2021, p. 10.17143.3.2. https://doi.org/10.7121/msi-eureka-10.17143.3.2.
[34] T. Pfullmann, P.A. Beaven, On the relationship between lattice parameters and composition of the γ-TiAl phase, Scr. Metall. Mater. 28 (3) (1993) 275–280, https://doi.org/10.1016/0956-716X(93)90427-T.
[35] E.S. Bumps, H.D. Kessler, M. Hansen, Titanium-aluminum system, JOM 4 (6) (1952) 609–614, https://doi.org/10.1007/BF03397728.
[36] M. Palm, L.C. Zhang, F. Stein, G. Sauthoff, Phases and phase equilibria in the Al-rich part of the Al–Ti system above 900 °C, Intermetallics 10 (6) (2002) 523–540, https://doi.org/10.1016/S0966-9795(02)00022-5.

[37] T.B. Massalski, H. Okamoto, P.R. Subramanian, L. Kacprzak. Binary Alloy Phase Diagrams, Second ed.,, ASM International, Materials Park OH,, USA, 1990.
[38] P. Hidnert, Thermal expansion of titanium, J. Res. Natl. Bur. Stand. 30 (1943) 101–105.
[39] D. Low, T. Sumii, M. Swain, Thermal expansion coefficient of titanium casting, J. Oral. Rehabil. 28 (3) (2001) 239–242, https://doi.org/10.1111/j.1365-2842.2001.00664.x.